



Paired metamorphism in the Neoproterozoic: A record of accretionary-to-collisional orogenesis in the North China Craton

Bo Huang^a, Timothy M. Kusky^{a,b,*}, Tim E. Johnson^{a,c}, Simon A. Wilde^c, Lu Wang^a, Ali Polat^{a,d}, Dong Fu^a

^a Center for Global Tectonics, School of Earth Sciences, State Key Laboratory of Geological Processes and Mineral Resources, China University of Geosciences, Wuhan 430074, China

^b Three Gorges Research Center for Geo-hazards, China University of Geosciences, Wuhan 430074, China

^c School of Earth and Planetary Sciences, Curtin University, Perth 6845, Australia

^d School of the Environment, University of Windsor, Windsor, ON N9B 3P4, Canada

ARTICLE INFO

Article history:

Received 4 February 2020

Received in revised form 16 May 2020

Accepted 20 May 2020

Available online xxx

Editor: A. Yin

Keywords:

paired metamorphism

plate tectonics

Archean

North China Craton

Dengfeng Complex

ABSTRACT

Paired metamorphism is the hallmark of asymmetric subduction at Phanerozoic convergent plate margins, yet spatially and temporally linked paired metamorphic belts have rarely been documented in the Archean rock record. Here, we investigate the Neoproterozoic Dengfeng Complex, a typical granite–greenstone belt in the southern part of the North China Craton (NCC). Using petrography, geochronology, and phase equilibrium constraints on rocks from different lithostructural units, we suggest the ca. 2.54–2.50-Ga Dengfeng Complex represents a remnant of a spatially and temporally linked Neoproterozoic paired metamorphic belt. In the western part of the complex, a garnet amphibolite from a dominantly metabasic unit (MBU) records near peak P – T conditions of 6.3–10 kbar and ~675–750 °C, corresponding to a high thermobaric ratio (T/P) of ~720–1200 °C/GPa. Tonalite–trondhjemite–granodiorite (TTG) gneisses preserve evidence for partial melting, also consistent with relatively high T/P (~875–1400 °C/GPa). In the eastern part of the Dengfeng Complex, two garnet amphibolites and three garnet quartz–mica schists from a dominantly metasedimentary unit (MSU) record peak P – T conditions of >9.8 kbar and ~525–655 °C, corresponding to intermediate thermobaric ratios of ~425–600 °C/GPa. Zircon and titanite U–Pb dating, coupled with existing ages of post-kinematic intrusions, constrain the metamorphic age to ca. 2.52–2.50 Ga. The metamorphic P – T data indicate that the MSU was buried to >30 km then exhumed to the near-surface by the early Paleoproterozoic. Our metamorphic results, when combined with recent structural and geochemical data, suggest the Dengfeng Complex records Neoproterozoic paired metamorphism, in which the higher thermal gradients reflect the arc–forearc region and the lower thermal gradients correspond to the accretionary complex. Our data indicate that the southern NCC experienced accretionary-to-collisional orogenesis with intra-oceanic subduction, forearc accretion (ca. 2.54–2.50 Ga), and subsequent arc–continent collision (ca. 2.50–2.47 Ga). The recognition of paired metamorphism in the NCC is consistent with widespread subduction and the operation of a plate tectonic regime in the late Archean.

© 2020 Elsevier B.V. All rights reserved.

1. Introduction

The tectonic regimes that operated in the Archean, and the processes responsible for producing the granite–greenstone belts that dominate Archean cratons, are hotly debated (e.g., Arndt, 2013; Béard, 2018; Kusky and Polat, 1999; Smithies et al., 2018). Two

major models have been proposed to explain the generation of Archean continental crust. Firstly, some form of subduction, perhaps related to a global plate tectonic regime, based on similarities with the ocean plate stratigraphy and geochemistry of modern accretionary complexes and/or oceanic lithosphere (e.g., Kusky et al., 2018; Polat et al., 2015). Alternatively, non-uniformitarian (pre-plate tectonic) modes that invoke melting near the base of oceanic plateaus, with or without plume tectonics, under a stagnant lid regime, including episodic crustal delamination and mantle overturns, based in part on the generalized dome-and-keel structure of some cratons and the predictions of geodynamic numerical mod-

* Corresponding author at: Center for Global Tectonics, School of Earth Sciences, State Key Laboratory of Geological Processes and Mineral Resources, China University of Geosciences, Wuhan 430074, China.

E-mail address: tkusky@gmail.com (T.M. Kusky).

elling (e.g., Johnson et al., 2014; Sizova et al., 2015; Van Kranendonk et al., 2014). The debate is closely related to the timing of emergence and subsequent evolution of plate tectonics on Earth (e.g., Cawood et al., 2018; Korenaga, 2013; Stern, 2018; Turner et al., 2020; Webb et al., 2020). An important question is how to recognize reliable evidence in the rock record that might signify the operation of the plate tectonic regime.

There is a great disparity in interpretations of how far back in the geological record plate tectonics can be traced, ranging from about 4.0 Ga, the age of the oldest rocks (e.g., Kusky et al., 2018; Turner et al., 2020), to the late Archean or Paleoproterozoic (e.g., Brown and Johnson, 2018; Cawood et al., 2018; Johnson et al., 2019), or even Neoproterozoic (e.g., Stern, 2018). Recent reviews incorporating geological and geochemical data from both igneous and sedimentary rocks suggest that a significant transition from a pre-plate tectonic mode to a self-sustaining plate tectonic regime occurred by the mid- to late Archean (e.g., Cawood et al., 2018; Johnson et al., 2019; Moyen and Laurent, 2018; Tang et al., 2016). However, a major argument against the emergence of plate tectonics in the Archean is the absence of modern-day petrological indicators of subduction, such as lawsonite-blueschist and ultra-high pressure metamorphic rocks that are widespread only since the Neoproterozoic (e.g., Stern, 2018). Rare examples of Paleoproterozoic rocks recording low geothermal gradients (François et al., 2018; Ganne et al., 2011; Glassley et al., 2014; Weller and St-Onge, 2017; Xu et al., 2018) provide strong evidence in favour of (cold) subduction or collision at that time, although whether these are of local or global significance is unclear. Brown and Johnson (2018, 2019) documented the secular change in thermobaric ratios (T/P) of global metamorphic rocks and noted the widespread appearance of rocks recording both high T/P ($>775^\circ\text{C}/\text{GPa}$, approximately equivalent to a geothermal gradient of $>24^\circ\text{C}/\text{km}$ assuming lithostatic pressure, mean $\sim 1100^\circ\text{C}/\text{GPa}$) and intermediate T/P metamorphism ($375\text{--}775^\circ\text{C}/\text{GPa}$, $\sim 12\text{--}24^\circ\text{C}/\text{km}$, mean $\sim 575^\circ\text{C}/\text{GPa}$) at the end of the Mesoarchean (<2800 Ma), which they interpreted to reflect the emergence of paired metamorphism and global plate tectonics; while the widespread appearance of low T/P metamorphism ($<375^\circ\text{C}/\text{GPa}$, $<12^\circ\text{C}/\text{km}$, mean $\sim 255^\circ\text{C}/\text{GPa}$) since the Neoproterozoic resulted from cold subduction–collision.

The classic view of paired metamorphic belts refers to the orogen-parallel, contemporaneous *in situ* metamorphic belts characterized by inboard high thermal gradients (high T/P) and outboard low thermal gradients (low T/P) in Pacific-type accretionary orogens (Miyashiro, 1961). Brown (2010) extended the concept of paired metamorphic belts to characterise tectonically juxtaposed metamorphic belts with higher (high T/P) and lower (low-to-medium T/P) thermal gradients in subduction-to-collision orogens, which appears more useful in gaining a better understanding of the relationship between thermal gradients and tectonic settings in ancient orogenic belts. Whereas many geochemical and geological features are controversial as indicators of geodynamic setting, the recognition of paired metamorphism in ancient rocks, reflecting a duality of thermal gradients associated with the subduction zone (low to intermediate T/P) and arc–backarc (high T/P) is widely regarded as a reliable indicator of subduction–collision (Brown, 2010; Brown et al., 2020; Holder et al., 2019; Miyashiro, 1961; Zheng and Zhao, 2020). However, few, if any, such spatially and temporally linked paired metamorphic belts have been well documented from Archean granite–greenstone terranes.

The Dengfeng Complex is a typical granite–greenstone belt in the southern segment of the Central Orogenic Belt of the North China Craton (NCC), comprising tonalite–trondhjemite–granodiorite (TTG) gneisses and metavolcano–sedimentary sequences (Diwu et al., 2011; Kröner et al., 1988; Zhang et al., 1985). The metavolcano–sedimentary assemblage was previously suggested to represent a sequence of continental rift-related rocks that developed in a

dome-and-keel like setting (Kröner et al., 1988; Zhang et al., 1985). However, more recent geochronological and geochemical studies have proposed that the TTG and mafic rocks formed at a convergent plate margin (Deng et al., 2016; Diwu et al., 2011; Wang et al., 2017). Further, field and structural data suggest that the Dengfeng greenstone belt constitutes a Neoproterozoic subduction–accretion complex in the east, and a dismembered intra-oceanic arc–forearc complex in the west (Huang et al., 2019). If these rocks formed in a subduction–collision setting, then paired metamorphism might be expected in the arc–forearc region (higher T/P) and forearc accretionary wedge (lower T/P), respectively. However, there were no comprehensive metamorphic data from the Dengfeng Complex to test this hypothesis. Similar controversies regarding non-plate or plate tectonic models for producing Archean granite–greenstone belts elsewhere are longstanding and ongoing (e.g., Kusky et al., 2018; Smithies et al., 2018; Webb et al., 2020). The Dengfeng Complex therefore provides an opportunity to examine contrasting geodynamic modes in the Neoproterozoic—an important transitional period in Earth's geodynamic evolution (e.g., Cawood et al., 2018; Brown et al., 2020).

Here, we integrate petrography, zircon and titanite U–Pb dating, with quantitative phase equilibrium modelling of metabasites, metapelites, and felsic gneisses from different lithostructural units of the Dengfeng Complex in order to reconstruct their metamorphic P – T – t evolution. Our new metamorphic data suggest that a Neoproterozoic paired metamorphic belt with distinct thermal gradients exists in the Dengfeng Complex, thus providing important insights into the tectonic evolution of the NCC and the prevailing geodynamic regime during the late Archean.

2. Geological background

The NCC contains a large area of Archean–Paleoproterozoic crust, comprising TTG gneisses, metamorphosed ultramafic to felsic intrusive and extrusive rocks, and metasedimentary strata (see Kusky et al., 2016 for a detailed summary). According to differences in the basement rocks, the NCC is generally subdivided into three major tectonic units (Fig. 1a), comprising the Eastern and Western blocks that are separated by a central orogenic belt that is termed either the Central Orogenic Belt (e.g., Kusky et al., 2016) or the Trans-North China Orogen (e.g., Zhao et al., 2005), depending on whether it formed in the Archean or Paleoproterozoic, respectively. The Paleoproterozoic Inner Mongolia–North Hebei Orogen occurs along the northern margin of the NCC (Kusky et al., 2016).

The Eastern Block is dominated by Eoarchean–Neoproterozoic (ca. 3.8–2.5 Ga) TTG gneisses and Neoproterozoic volcano–sedimentary sequences (Zhao et al., 2005). The basement of the Western Block, which has a thick cover of Mesozoic sedimentary rocks, comprises Archean–Paleoproterozoic rocks (Zhao et al., 2005). The Central Orogenic Belt is mainly composed of low- to high-grade metamorphic complexes (Fig. 1b), including Neoproterozoic to Paleoproterozoic TTG gneisses, granulites, metavolcano–sedimentary rocks, granitoids, and Paleoproterozoic sedimentary sequences (Kusky et al., 2016; Zhao et al., 2005). Two episodes of metamorphism with peak ages of ca. 1.85 Ga and ca. 2.50 Ga have been recognized (e.g., Zhang et al., 2020). The younger high-grade episode (1.95–1.80 Ga) records collision and cratonization, although whether this was related to collision between the Eastern and Western blocks (e.g., Zhao et al., 2005), or between the NCC and the supercontinent Columbia to the north (Kusky et al., 2016) is debated. Hence, deciphering the P – T – t evolution of the Neoproterozoic metamorphism may provide important constraints on the earlier tectonic history of the NCC, which is largely overprinted by Paleoproterozoic and Mesozoic tectonism and metamorphism.

The Dengfeng Complex in the southern NCC consists of TTG gneisses, metavolcano–sedimentary rocks, metadiorite, and post-

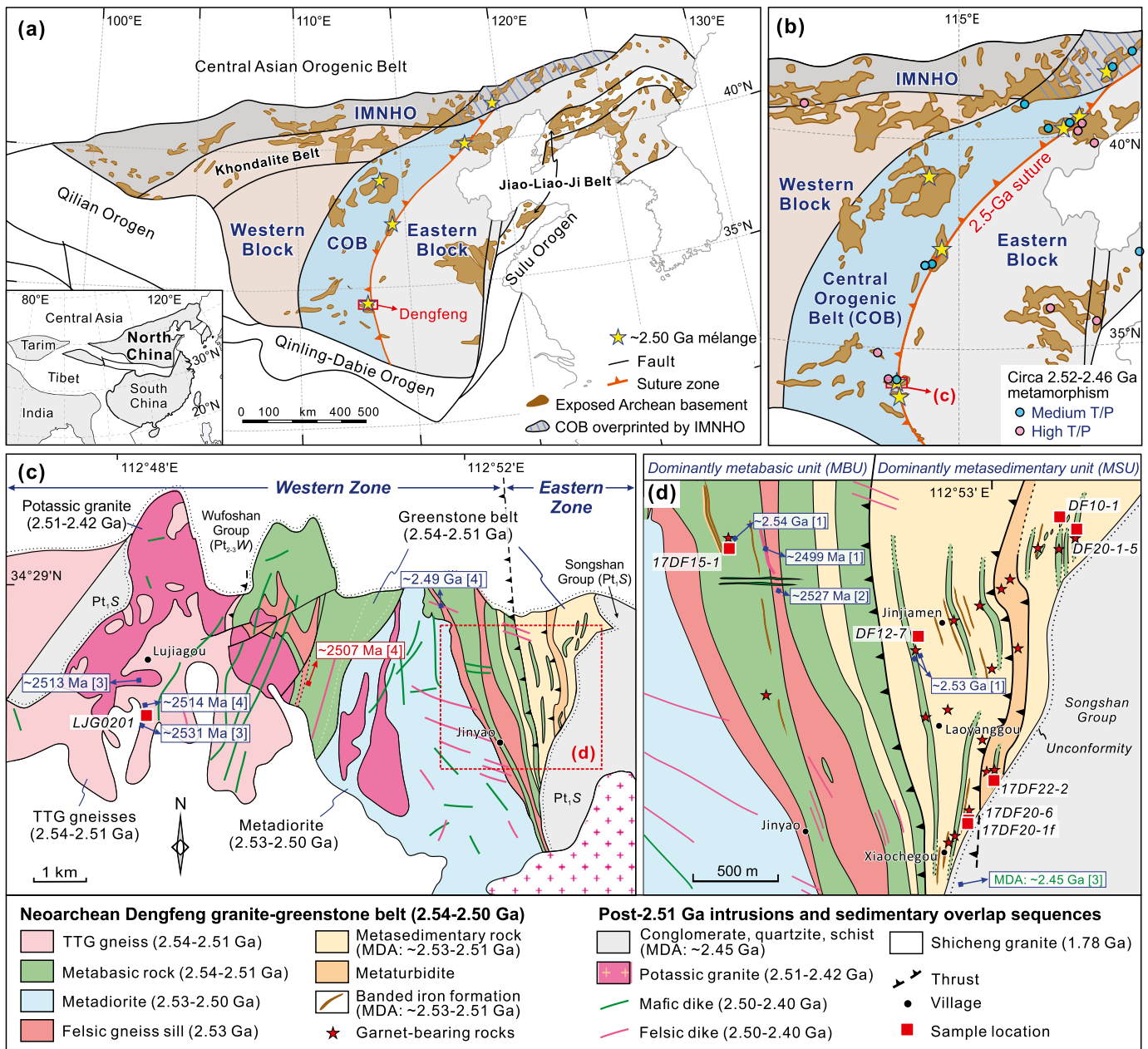


Fig. 1. (a–b) Simplified geological map showing tectonic units of the NCC (modified after Kusky et al., 2016). According to the division schemes of the NCC by Kusky et al. (2016), the major tectonic units include the Archean Eastern and Western blocks, the Neoarchean Central Orogenic Belt (COB), and the Paleoproterozoic Inner Mongolia-North Hebei Orogen (IMNHO). The boundaries of the Jiao-Liao-Ji Belt and the Khondalite Belt are shown (after Zhao et al., 2005). (c) Geological map of the Dengfeng Complex (modified after Zhang et al., 1985; Huang et al., 2019). (d) Detailed geological map showing the metavolcano-sedimentary assemblage and sample locations used in this study (after Huang et al., 2019). Two lithostructural units, including a dominantly metabasic unit (MBU) and a dominantly metasedimentary unit (MSU) in the east (Huang et al., 2019). These two units are characterized by different lithological associations, metamorphic patterns and structural styles, and are separated by top-to-the-northeast thrust faults and shear zones (Huang et al., 2019). The MBU consists predominantly of amphibolite and garnet amphibolite with minor quartz-rich schists and banded iron formations (BIFs). The amphibolites have tholeiitic major-element compositions and trace element characteristics similar to mid-ocean ridge basalt (MORB) and island arc tholeiite (IAT) (Deng et al., 2016; Diwu et al., 2011). Zircon U–Pb age data indicate that the amphibolite protolith formed at ca. 2.54 Ga and experienced metamorphism at 2.51–2.50 Ga (Deng et al., 2016; Diwu et al., 2011; Huang et al., 2019). Circa 2.53 Ga granitic sills/dikes that intrude the metabasic unit have adakite-like geochemical compositions (Wang et al., 2017). The MSU in the eastern part of the Dengfeng greenstone belt is dominated by metapelite (quartz–mica schist), metaconglomerate, metagraywacke, with minor amphibolite and BIF (Huang et al., 2019). Three discrete lithologic associations can be recognized and comprise a coherent schist–amphibolite sequence, a metatur-

kinematic granitic and mafic intrusions (Fig. 1c, d). The meta-volcano-sedimentary assemblage, known as the Dengfeng greenstone belt, can be subdivided into two lithostructural units; a dominantly metabasic unit (MBU) in the west, and a dominantly metasedimentary unit (MSU) in the east (Huang et al., 2019). These two units are characterized by different lithological associations, metamorphic patterns and structural styles, and are separated by top-to-the-northeast thrust faults and shear zones (Huang et al., 2019). The MBU consists predominantly of amphibolite and garnet amphibolite with minor quartz-rich schists and banded iron formations (BIFs). The amphibolites have tholeiitic major-element compositions and trace element characteristics similar to mid-

ocean ridge basalt (MORB) and island arc tholeiite (IAT) (Deng et al., 2016; Diwu et al., 2011). Zircon U–Pb age data indicate that the amphibolite protolith formed at ca. 2.54 Ga and experienced metamorphism at 2.51–2.50 Ga (Deng et al., 2016; Diwu et al., 2011; Huang et al., 2019). Circa 2.53 Ga granitic sills/dikes that intrude the metabasic unit have adakite-like geochemical compositions (Wang et al., 2017).

The MSU in the eastern part of the Dengfeng greenstone belt is dominated by metapelite (quartz–mica schist), metaconglomerate, metagraywacke, with minor amphibolite and BIF (Huang et al., 2019). Three discrete lithologic associations can be recognized and comprise a coherent schist–amphibolite sequence, a metatur-

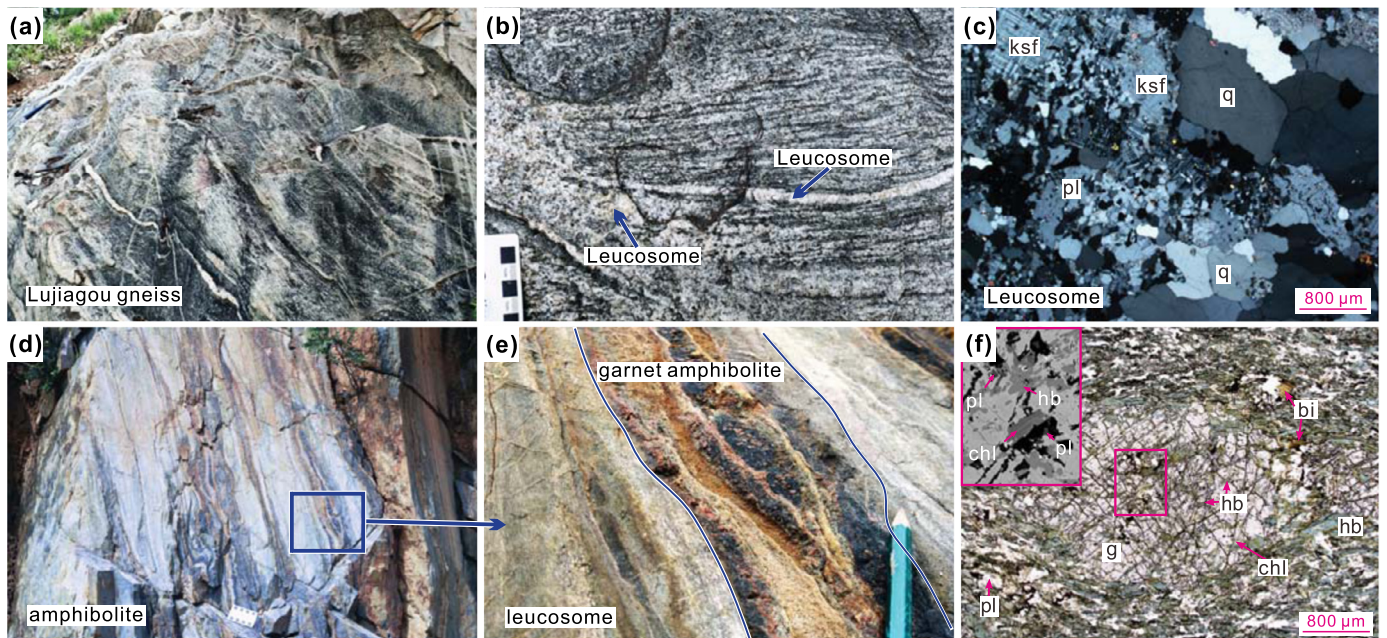


Fig. 2. Field photographs and photomicrographs of migmatized tonalitic gneisses and metabasic rocks in the western part of the Dengfeng Complex (Western Zone). (a–b) Intensely migmatized TTG gneisses at Lujiagou, with abundant leucosome veins. (c) Leucosome in the Lujiagou tonalitic gneiss; cross-polarized light. (d–e) Garnet amphibolite in a high-strain zone in the dominantly metabasic unit. (f) Sample 17DF15-1, garnet amphibolite, a garnet (g) porphyroblast contains inclusions of hornblende (hb)–plagioclase (pl)–ilmenite (ilm)–quartz (q); hornblende–plagioclase–minor biotite (bi) is present in the matrix; chlorite (chl) occurs along cracks in garnet and the matrix.

bidite unit, and a chaotic schist–amphibolite unit. The chaotic schist–amphibolite assemblage has typical block-in-matrix fabrics and duplex structures, features similar to Phanerozoic mélanges (Huang et al., 2019). A variety of blocks and boudins, including amphibolite, garnet amphibolite, granite, and Fe-rich quartzite, are enclosed in strongly-deformed quartz-rich schists. The protoliths of the metabasite blocks are interpreted to have been mid ocean ridge basalt (MORB)- or island arc-tholeiite (IAT)-like basaltic rocks based on their major and trace element compositions (Huang et al., 2019), whereas the metasedimentary matrix likely represents metamorphosed pelagic–hemipelagic siliceous to argillaceous sediments. Zircon U–Pb ages indicate that the amphibolites formed at ca. 2.54 Ga and the sedimentary rocks have maximum depositional ages ranging from ca. 2.53 Ga to 2.51 Ga (Huang et al., 2019; Wan et al., 2009).

The TTG and granitic rocks mainly crop out along the western margin (Lujiagou area) of the Dengfeng Complex (Fig. 1c). The TTG gneisses have zircon U–Pb ages of 2.54–2.51 Ga, and were interpreted as intra-oceanic arc complexes (Deng et al., 2016; Diwu et al., 2011). Potassic granites and leucogranitic veins in the Lujiagou area (Fig. 1c) have zircon U–Pb ages ranging from ca. 2.51 Ga to 2.42 Ga. Geochemical and isotopic data suggest they were generated by partial melting of the TTG rocks (Wan et al., 2009; Zhou et al., 2011). The TTG rocks to the east of the MSU are significantly older with zircon U–Pb ages of 2.66–2.55 Ga, and are interpreted as the basement rocks of the Eastern Block of the NCC (Huang et al., 2019). A high-Mg metadiorite that intruded the central part of the greenstone belt has a sanukitoid-like composition and a crystallization age of 2.53–2.50 Ga, but contains leucogranitic veins that record anatexis at ca. 2.47 Ga (Deng et al., 2016, 2019; Diwu et al., 2011). Numerous 2.50–2.40 Ga granitic and mafic dikes intrude the TTGs and metavolcano-sedimentary assemblages (Deng et al., 2016, 2019; Huang et al., 2019).

In a recent geodynamic model largely based on geochemical data and structural zonation, the ca. 2.54–2.51-Ga TTG gneisses and coeval MBU in the west (referred to as the Western Zone, Fig. 1c) were interpreted as an arc–forearc assemblage formed in the upper plate, whereas the coeval MSU in the east (East-

ern Zone) was interpreted as the accretionary complex derived from the lower plate (Huang et al., 2019). Here, we examine the metamorphic patterns of representative rocks from these units to test the viability of this hypothesis. Sample localities are shown in Fig. 1c–d.

3. Field and petrographic observations

3.1. TTG and amphibolites within the Western Zone

Tonalitic gneisses in the western part of the Dengfeng Complex are intensely migmatized and deformed and contain abundant leucosome veins and dikes (Fig. 2a, b). The tonalitic gneisses are composed of plagioclase (~60 vol.%), quartz (~20 vol.%), biotite (~10 vol.%), hornblende (~10 vol.%), with accessory titanite. The leucosomes and leucogranitic dikes are composed of quartz, plagioclase, and K-feldspar, with minor titanite (Fig. 2c). A migmatitic tonalitic gneiss sample (JLG0201) was collected for zircon U–Pb dating (Fig. 1c).

Most amphibolites within the MBU are foliated, although in some low-strain zones magmatic structures are preserved (Huang et al., 2019). Garnet amphibolite occurs along high-strain zones that are characterized by a pervasive foliation and they preserve evidence of partial melting (Fig. 2d). Leucosome veins are up to 15 cm wide and composed of quartz and plagioclase, with minor hornblende and Fe-oxide. A sample of garnet amphibolite (17DF15-1, Fig. 1d) containing abundant garnet porphyroblasts (Fig. 2e) was collected for phase equilibrium modelling and U–Pb dating of zircon and titanite. It consists of hornblende (~65% vol.%), plagioclase (~15 vol.%), garnet (~10 vol.%), chlorite (~2 vol.%), quartz (~4 vol.%), and biotite (~1 vol.%) (Fig. 2f), with accessory ilmenite, magnetite and titanite. Hornblende, plagioclase, quartz, and ilmenite within garnet porphyroblasts might be mineral inclusions and/or may have formed later along fractures. The matrix minerals are hornblende, plagioclase, and quartz, with minor biotite, ilmenite and titanite. Hornblende and plagioclase replace garnet porphyroblasts at their margins and along fractures.

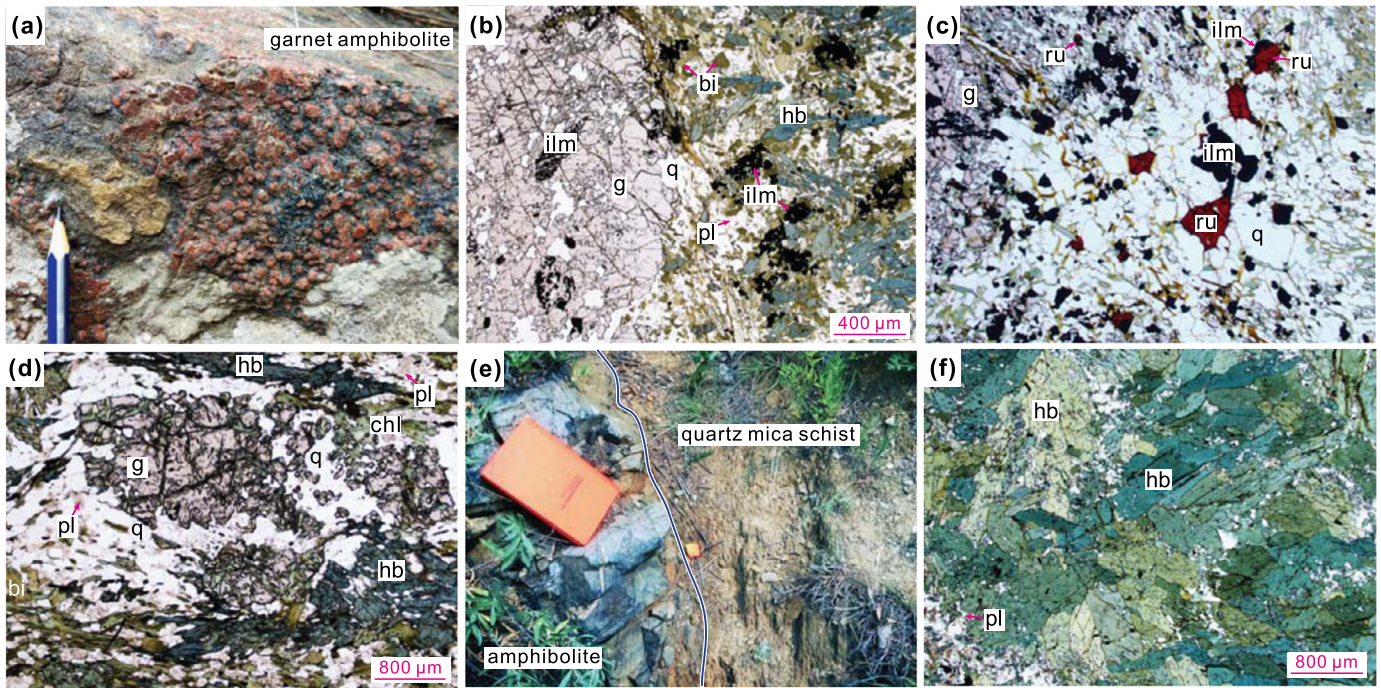


Fig. 3. Field photographs and photomicrographs of metabasic rocks in the dominantly metasedimentary unit (MSU), eastern Dengfeng Complex. (a) Garnet amphibolite block. (b–c) Sample DF20-1-5, garnet amphibolite, a mega-garnet porphyroblast surrounded by hornblende, plagioclase, biotite, ilmenite, rutile, and quartz; plane-polarized light. (d) Sample 17DF22-2, garnet amphibolite, a garnet porphyroblast surrounded by hornblende, plagioclase, quartz, ilmenite, and chlorite; plane-polarized light. (e) Amphibolite block in quartz-mica schist matrix. (f) Sample DF10-1, portion of a garnet-free amphibolite block in a schist matrix; plane-polarized light. Mineral abbreviations as in Fig. 2.

3.2. Amphibolite and metapelite within the Eastern Zone

The MSU mainly consists of diverse metasedimentary rocks with minor metabasic rocks (amphibolite and garnet amphibolite) (Fig. 3a, e) that occur as sheets and centimeter- to meter-sized lenses or blocks within the metasedimentary matrix (Fig. 3e). Representative samples were collected for phase equilibrium modelling and/or zircon U–Pb dating, including two garnet amphibolites (DF20-1-5; 17DF22-2), a garnet-free amphibolite (DF10-1), and three garnet-bearing quartz–mica schists (DF12-7, 17DF20-6, 17DF20-1f). The locations of the samples are shown in Fig. 1d.

Garnet amphibolite sample DF20-1-5 is composed of hornblende (~40 vol.%), garnet (~30 vol.%), biotite (~15 vol.%), quartz (~9 vol.%), plagioclase (~2 vol.%), chlorite (~1 vol.%), epidote (~1 vol.%), and ilmenite (~2 vol.%), with accessory rutile, and titanite (Fig. 3b). Garnet porphyroblasts (~1.5–5 mm in diameter) contain inclusions of quartz and ilmenite (Fig. 3b). Accessory rutile occurs in the matrix (Fig. 3c). Garnet amphibolite sample 17DF22-2 is composed of hornblende (~30 vol.%), biotite (~20 vol.%), garnet (~15 vol.%), plagioclase (~20 vol.%), quartz (8 vol.%), chlorite (~2 vol.%), ilmenite (~1 vol.%), and minor rutile. Some thinly-banded quartz veins also occur in the sample. Hornblende–plagioclase–ilmenite symplectites surround embayed garnet at its margins (Fig. 3d). Chlorite within the matrix and along fractures in garnet is interpreted to be a retrograde mineral. The garnet-free amphibolite sample (DF10-1) is weakly-deformed and composed predominantly of hornblende with minor epidote, biotite, plagioclase, Fe-oxide, and titanite (Fig. 3f).

The garnet-bearing metapelites are strongly foliated, with some showing compositional variations in which Al-rich layers contain abundant garnet porphyroblasts (Fig. 4a, b). Two samples (17DF20-6 and 17DF20-1f) from different layers within the same outcrop were chosen for phase equilibria modelling. Most garnet quartz–mica schists have a pervasive foliation defined by muscovite, chlorite and quartz, and contain strongly-deformed garnet porphyroblasts with asymmetric S–C, sigma, or snowball fabrics (Fig. 4c, g).

The long axes of garnets are mostly parallel to the penetrative foliation and preserve evidence of shearing.

Metapelite sample 17DF20-6 is composed of quartz (~35 vol.%), garnet (~15 vol.%), muscovite (~25 vol.%), plagioclase (~15 vol.%), chlorite (~3 vol.%), biotite (~1 vol.%), epidote (~1 vol.%), ilmenite (~1 vol.%), and minor rutile (Fig. 4c–f). The garnet porphyroblasts exhibit zoning with relatively euhedral cores and deformed rims (Figs. 4e and S1a–c). Most garnet porphyroblasts contain abundant quartz inclusions (~5–20 μm) in their cores. Rarely, an inclusion assemblage of chloritoid–muscovite–biotite–chlorite–quartz–ilmenite–epidote is preserved in the garnet cores (Fig. 4f). Rutile mainly occurs in the matrix as elongate grains, some of which are partially replaced by ilmenite (Figs. 4d and S1d). Biotite is idioblastic to subidioblastic, and commonly cross-cuts the foliation (Fig. 4e). Epidote occurs as inclusions within biotite and garnet. From the same outcrop, sample 17DF20-1f is composed of quartz (~20 vol.%), garnet (~40 vol.%), muscovite (~35 vol.%), chlorite (~3 vol.%), ilmenite (~2 vol.%), and minor rutile (Fig. 4g, h). Quartz and muscovite define the strong foliation. Sample DF12-7, from a separate outcrop about 900 meters away (Fig. 1d), is associated with garnet-free quartz-rich schists and garnet amphibolites. The mineral assemblage is garnet (~25 vol.%), quartz (~40 vol.%), plagioclase (~25 vol.%), biotite (~3 vol.%), muscovite (~2 vol.%), chlorite (~2 vol.%), and ilmenite (~0.5 vol.%), with accessory rutile and apatite (Fig. 4i).

4. Methods

Compositional analyses, backscattered electron (BSE) images of representative minerals and X-ray compositional mapping were undertaken on a JEOL JXA 8230 electron probe micro-analyser (EPMA) in the Center for Global Tectonics at the School of Earth Sciences, China University of Geosciences, Wuhan. Zircon and titanite were analyzed using either a sensitive high-resolution ion

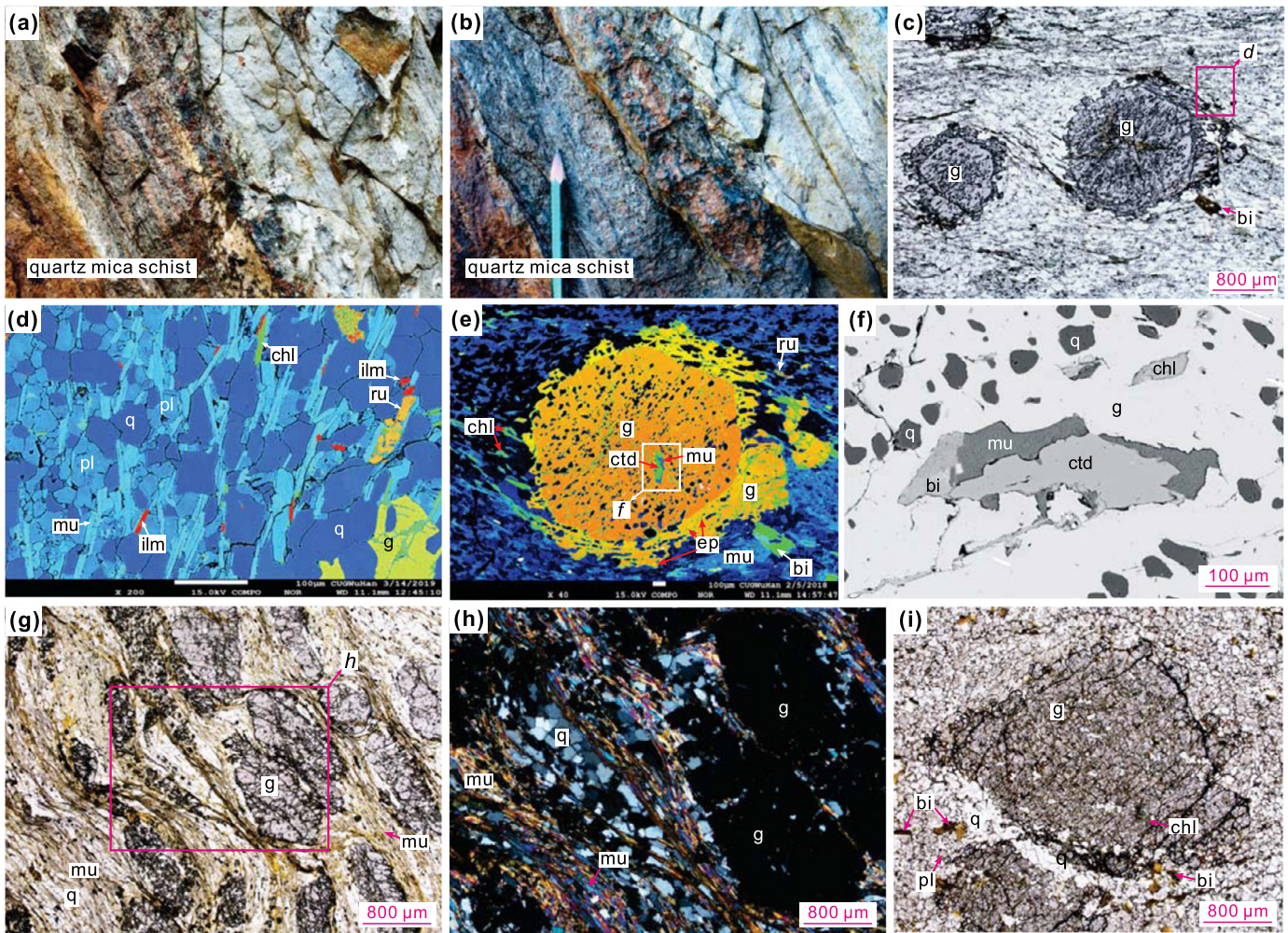


Fig. 4. Images showing the mineral assemblages and textures of metapelites from the MSU, eastern Dengfeng Complex. (a–b) Field photographs of quartz-mica schist showing garnet-rich and garnet-free zones; (c) Sample 17DF20-6, Garnet quartz-mica schist with garnet porphyroblasts and a matrix of quartz-muscovite (mu)-chlorite-ilmenite-rutile (ru)-biotite; plane-polarized light; (d) Colour back-scattered electron (BSE) image showing matrix assemblage of quartz-muscovite-plagioclase-ilmenite-rutile-chlorite in sample 17DF20-6; (e–f) BSE images showing inclusions of chloritoid (ctd)-muscovite-biotite-quartz-chlorite in a garnet porphyroblast in sample 17DF20-6. (g) Sample 17DF20-1f, garnet quartz-mica schist, with strongly deformed garnet porphyroblasts parallel to the foliated matrix assemblage of quartz-muscovite-rutile-ilmenite-chlorite; plane-polarized light; (h) similar to (g) but in cross-polarized light; (i) Sample DF12-7, garnet-bearing quartz schist with quartz, plagioclase, and minor biotite in the matrix; plane-polarized light. Mineral abbreviations as in Fig. 2.

microprobe (SHRIMP II) or by LA-ICP-MS at the John de Laeter Centre, Curtin University, Perth, Australia. A detailed description of the analytical methods can be found in the Supplementary Text. Representative mineral compositions, X-ray maps, compositional diagrams, and descriptions are presented in the supplementary materials; zircon and titanite U–Pb isotopic data are listed in Supplementary Tables S2–3.

Phase equilibrium modelling (P – T pseudosection) calculations were performed using THERMOCALC 3.45 (Powell and Holland, 1988) in the Na_2O – CaO – K_2O – FeO – MgO – Al_2O_3 – SiO_2 – H_2O – TiO_2 – O (NCKFMASHTO) system using the ds62 internally consistent end-member thermodynamic data set (Holland and Powell, 2011). The bulk-rock compositions (Table S4) used in construction of the diagrams were based on XRF analyses, for which CaO contents were adjusted according to the measured P_2O_5 contents to account for the presence of apatite, the only P-bearing phase in the samples. In all samples, Mn contents were low (<0.1 wt.%) and were not included in the calculations. Values of $X(\text{Fe}^{3+})$ [= atomic $\text{Fe}^{3+}/(\text{Fe}^{2+} + \text{Fe}^{3+})$] of 0.1 were used. The phases considered in the modelling and the corresponding activity–composition (a – x) models follow White et al. (2014) and Green et al. (2016). Quartz, albite, sphene (titanite), rutile, sillimanite, and aqueous fluid (H_2O) were

treated as pure end-member phases. Mineral abbreviations used in the P – T pseudosections are from Holland and Powell (2011). Assemblage fields and P – T ranges consistent with the inferred peak assemblage are outlined in Fig. 5; see supplementary Figs. S6–S8 and Text for more details. For comparison, we estimated the approximate P – T conditions of some samples using those mineral compositions interpreted to reflect peak or retrograde conditions in conjunction with the average- PT (AvPT) mode of THERMOCALC and conventional geothermobarometers (Table S5), following the methods described in Huang et al. (2019).

5. Results

5.1. Phase equilibria modelling

5.1.1. Western Zone

Based on the average composition of tonalitic gneisses in the western part of the Dengfeng Complex (Diwu et al., 2011; Deng et al., 2016), we modelled the P – T conditions of partial melting of the gneisses (Fig. S6), assuming an H_2O content producing minimal H_2O -saturated melting at 7 kbar. A P – T range of <10.5 kbar and 640–810 °C is predicted based on the mineral assemblages, which

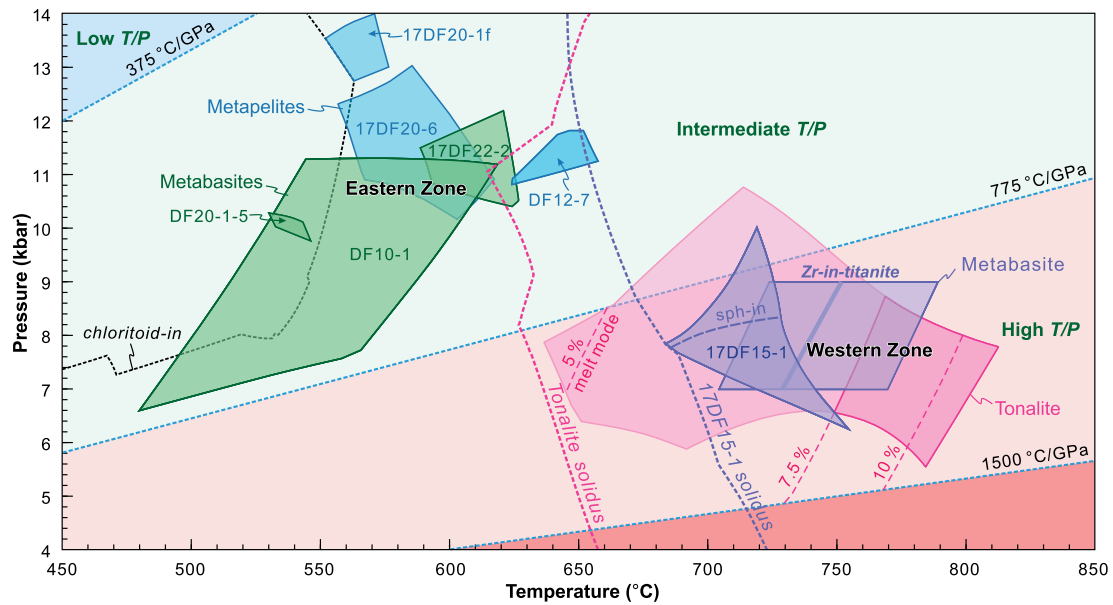


Fig. 5. Summary of estimated peak P - T fields of representative rocks by pseudosections from the Dengfeng Complex. The inferred peak P - T ranges of metapelites and metabasites from the dominantly metasedimentary unit (MSU) in the eastern part of the Dengfeng Complex correspond to intermediate T/P thermal gradients. The pink field represents the P - T range for the partial melting of the tonalitic gneisses in the Lujiagou area, western Dengfeng Complex. The preferred peak P - T conditions are bounded by bold pink lines, at which the proportion of melt is $>7.5\%$. The purple field represents the peak P - T range of partially molten amphibolite from the dominantly metabasic unit (MBU), western Dengfeng Complex. The chloritoid-in line was based on the pseudosection of metapelite sample 17DF20-1f. Zr-in-titanite represents estimated temperatures for sample 17DF15-1 using Zr-in-titanite thermometry. Pseudosections and detailed descriptions for all samples can be found in supplementary Figs. S6–8 and Text.

lack garnet, rutile and orthopyroxene (Fig. 5). However, based on the proportion of leucosome in the rocks (Fig. 2a, b), we estimate minimum melt fractions of 7.5 vol.%, consistent with minimum temperatures of ~ 750 – 810 °C and pressures of 5.6–8.8 kbar (Fig. 5).

A P - T pseudosection from 4 to 13 kbar and 400 to 800 °C for amphibolite sample 17DF15-1, with an H_2O content assuming minimal H_2O -saturated melting, is shown in Fig. S7a. The calculated solidus is located at ~ 650 – 720 °C above 4 kbar. The absence of augite in this sample provides a conservative higher temperature limit, as all clinopyroxene may have been replaced by hornblende on re-crossing the solidus. Some titanite grains contain inclusions of hornblende and chlorite, and likely formed during prograde metamorphism. However, whether titanite was present at the peak condition or not cannot be determined. The inferred peak mineral assemblage of garnet–hornblende–quartz–plagioclase–melt, with or without titanite, implies pressures of 6.3–10 kbar and temperatures of 675–750 °C (Fig. 5). The retrograde assemblage of hornblende–plagioclase–biotite–chlorite–ilmenite is stable over a P - T range of <7.6 kbar and ~ 460 – 500 °C.

5.1.2. Eastern Zone

In the P - T pseudosection for garnet amphibolite sample DF20-1-5 (Fig. S7b), the stability field for the inferred peak assemblage of garnet–hornblende–biotite–epidote–chlorite–rutile \pm ilmenite and quartz, occurs at >9.8 kbar and 525–545 °C (Fig. 5), although muscovite, which is predicted to be present in these fields, is not observed in the sample. For garnet amphibolite sample 17DF22-2 (Fig. S7c), the stability field for the interpreted peak assemblage of garnet–hornblende–plagioclase–biotite–rutile \pm ilmenite–quartz occurs over a narrow P - T range of 10.4–12.0 kbar and 590–625 °C (muscovite is not observed, Fig. 5). Sample 17DF22-2 yields P - T conditions of ~ 10.3 kbar and ~ 562 °C for garnet rims using garnet–biotite–plagioclase–quartz (GBPQ) thermobarometry (Wu et al., 2004), and $\sim 550 \pm 17$ °C/ 9.7 ± 0.7 kbar using the average P - T mode of THERMOCALC (Table S5). In the P - T pseudosection for garnet-free amphibolite sample DF10-1 (Fig. S7d), the

stability field for the interpreted peak assemblage of hornblende–epidote–biotite–titanite–quartz occurs over a large P - T range of 6.6–11.4 kbar and 480–630 °C (Fig. 5). This sample yields P - T conditions of ~ 559 – 622 °C and ~ 9.8 – 10.7 kbar using hornblende–plagioclase–quartz (HPQ) thermobarometry.

Three P - T pseudosections from 2 to 14 kbar and 450 to 700 °C for three representative garnet quartz–mica schist samples are shown in Fig. S8. Paragonite is not considered in all samples due to infelicities in the white mica solution model. For sample 17DF20-6, the inferred peak assemblage of garnet–quartz–plagioclase/albite–muscovite–biotite–epidote \pm ilmenite–rutile is stable at pressures of >10.2 kbar and temperatures of ~ 555 – 615 °C (Fig. 5). For sample 17DF20-1f, the inferred peak assemblage of garnet–muscovite–chlorite \pm ilmenite–rutile \pm magnetite–quartz is stable at higher pressures of >12.5 kbar and temperatures of ~ 550 – 575 °C (Fig. 5). For sample DF12-7, the inferred peak assemblage of garnet–plagioclase–muscovite–biotite \pm ilmenite–rutile is stable at pressures of ~ 10.8 – 11.8 kbar and temperatures of ~ 620 – 655 °C (Fig. 5). The combined data for metapelite samples yield P - T conditions of ~ 8.9 – 9.7 kbar and ~ 520 – 550 °C using the average P - T mode of THERMOCALC (Table S5).

5.2. Zircon and titanite geochronology

Zircon grains from the migmatitic tonalitic gneiss LJG0201 from the Western Zone are subhedral to euhedral. Cathodoluminescence (CL) images (Fig. 6a) reveal some grains have homogeneous rims with high luminescence, consistent with a metamorphic origin. Five analyses of cores yield a weighted mean $^{207}\text{Pb}/^{206}\text{Pb}$ age of 2528 ± 13 Ma (2σ , MSWD = 0.11, Fig. 6a), interpreted as the crystallization age of the tonalite. Six analyses of rims yield a younger weighted mean $^{207}\text{Pb}/^{206}\text{Pb}$ age of 2518 ± 12 Ma (MSWD = 0.83, Fig. 6a), interpreted as the age of metamorphic recrystallization.

Zircon grains in amphibolite sample 17DF15-1 from the western Dengfeng Complex (MBU) are subhedral and stubby to prismatic. Cathodoluminescence images reveal two distinct internal

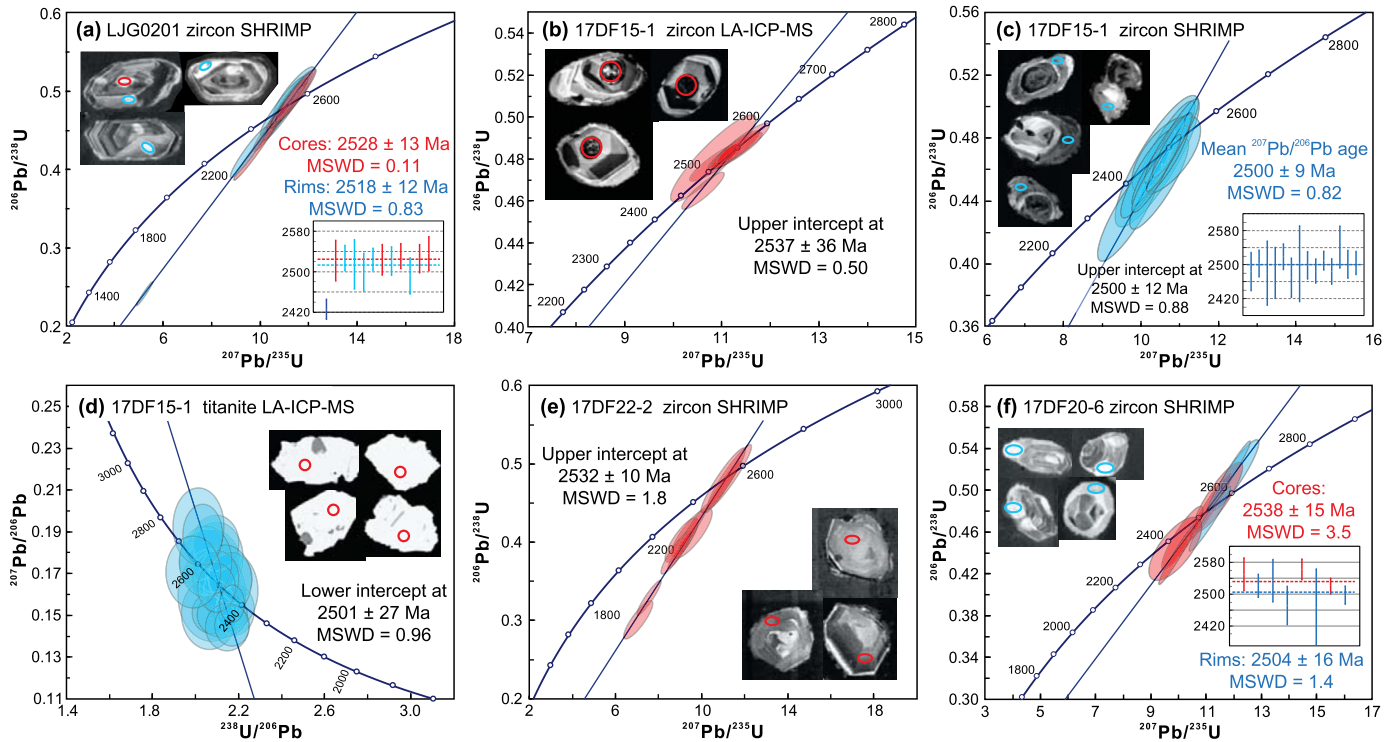


Fig. 6. Zircon and titanite U–Pb concordia diagrams with representative cathodoluminescence images of zircons and back-scattered electron images of titanite. (a) SHRIMP dating of zircons from sample LJG0201 (tonalitic gneiss). (b) LA-ICP-MS dating of zircon cores from sample 17DF15-1 (garnet amphibolite). (c) SHRIMP dating of zircon rims from sample 17DF15-1. (d) LA-ICP-MS dating of titanites from sample 17DF15-1. (e) SHRIMP dating of zircons from sample 17DF22-2 (garnet amphibolite). (f) SHRIMP dating of zircon rims from sample 17DF20-6 (metapelite). The SHRIMP and LA-ICP-MS analysis spots had diameters of 24 μm and 32 μm , respectively.

morphologies, in which oscillatory-zoned cores are overgrown by narrow metamorphic rims with either high or low luminescence (Fig. 6b–c). Six LA-ICP-MS analyses of zircon cores define an upper intercept age of 2537 ± 36 Ma (Fig. 6b). These analyses are associated with moderate to high Th/U ratios (0.17–0.89), positive Ce/Ce^* ($= \text{Ce}_N/\sqrt{(\text{La}^*\text{Pr})_N}$, where subscript N reflect normalisation to chondritic values (Sun and McDonough, 1989) and enrichment in heavy rare earth elements (HREEs) (Fig. S9a), consistent with a magmatic origin. Fourteen SHRIMP analyses (Table S2) on zircon rims yield a weighted mean $^{207}\text{Pb}/^{206}\text{Pb}$ age of 2500 ± 9 Ma (MSWD = 0.82, Fig. 6c). These analyses have extremely low Th/U ratios (0.002–0.06), consistent with a metamorphic origin.

Titanite grains in sample 17DF15-1 are mostly stubby prisms. On a Tera–Wasserburg plot, twenty-two LA-ICP-MS analyses define a discordia with a lower intercept age of 2501 ± 27 Ma (MSWD = 0.96, Fig. 6d). Based on chondrite-normalized rare earth element (REE) patterns (Fig. S9b), the titanite grains can be subdivided into four groups that have variable Eu/Eu^* ($= \text{Eu}_N/\sqrt{(\text{Sm}^*\text{Gd})_N}$) anomalies (Fig. S9e–f) and either depleted or enriched light rare earth element (LREE) and HREE patterns (Fig. S9b–c). Such complex REE characteristics imply that titanite may represent multiple growth populations that equilibrated with different minerals, in particular garnet and plagioclase. Using Zr-in-titanite thermometry for a given pressure and an activity of TiO_2 (a_{TiO_2}) of 0.5 (Hayden et al., 2008), the measured concentrations of Zr (177–558 ppm, average = 294 ppm) correspond to temperatures of 704–765 $^\circ\text{C}$ (average = 728 $^\circ\text{C}$) at a pressure of 7 kbar, and 727–789 $^\circ\text{C}$ (average = 751 $^\circ\text{C}$) at a higher pressure of 9 kbar (Table S3), for which estimated uncertainties are ± 20 $^\circ\text{C}$ (Hayden et al., 2008).

Zircon grains in amphibolite sample 17DF22-2 from the eastern Dengfeng Complex (MSU) are subhedral to euhedral, stubby to prismatic in shape and show sector or patchy zoning in CL images (Fig. 6e). SHRIMP analyses reveal variable concentrations

of Th (33–196 ppm) and U (72–388 ppm), and high Th/U ratios (0.36–0.95, Table S2). Eight analyses define a discordia with an upper intercept age of 2532 ± 10 Ma (MSWD = 1.8, Fig. 6e), interpreted as the crystallization age of the sample.

Zircon grains in metapelite sample 17DF20-6 from the eastern Dengfeng Complex (MSU) are irregular to euhedral in shape. In CL images, most grains preserve oscillatory zoning, although some exhibit core–rim structures with CL-brighter rims, consistent with a metamorphic origin. Analyses yield variable concentrations of Th (19–114 ppm) and U (53–118 ppm), and high Th/U ratios (0.20–1.00, Table S2). Three analyses on cores yield a weighted mean $^{207}\text{Pb}/^{206}\text{Pb}$ age of 2538 ± 15 Ma (MSWD = 3.5, Fig. 6f), whereas five analyses on rims yield a weighted mean $^{207}\text{Pb}/^{206}\text{Pb}$ age of 2504 ± 16 Ma (MSWD = 1.4, Fig. 6f), interpreted as the time of metamorphism.

6. Discussion

6.1. Metamorphic P – T evolution of the Dengfeng Complex

6.1.1. Higher T/P metamorphism

In the western part of the Dengfeng Complex, the TTG gneisses (2.54–2.51 Ga) and amphibolite within the MBU record intense migmatization. The early episode of anatexis (ca. 2.51 Ga) in the TTG rocks is coeval with that in the metabasites in the MBU. Phase equilibrium modelling of an average TTG from the western Dengfeng Complex indicates that partial melting was associated with a relatively high T/P of 875–1400 $^\circ\text{C}/\text{GPa}$. Similarly, garnet amphibolite sample 17DF15-1 from the MBU yields P – T conditions (Fig. 5) corresponding to a relatively high thermal gradient of 720–1200 $^\circ\text{C}/\text{GPa}$. If titanite is not included in the peak mineral assemblage, the resulting P – T range (6.3–8.4 kbar and 685–755 $^\circ\text{C}$) corresponds to a thermal gradient of 925–1200 $^\circ\text{C}/\text{GPa}$. Zr-in-titanite thermometry yields metamorphic temperatures of 728 $^\circ\text{C}$

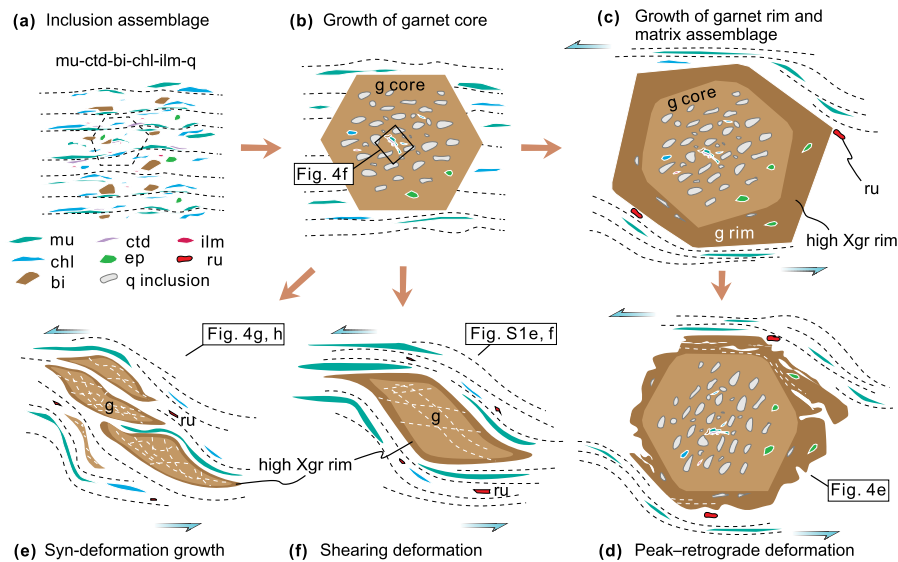


Fig. 7. Growth and deformation of garnet porphyroblasts in metapelites from the MSU, eastern Dengfeng Complex. (a–d) Prograde to peak and retrograde evolution and mineral assemblages based on sample 17DF20-6. Note that a chloritoid- and chlorite-bearing assemblage (a–b) is preserved in the cores of garnet, implying low- T and medium- P . Corresponding petrographic evidence is shown in Fig. 4f. The rims of garnet (c, e, f) show a significant increase of X_{gr} , implying an increase of pressure. Rutile (ru) in the matrix also supports relatively high- P . (e–f) Deformed and dismembered garnet porphyroblasts resulted from strong shearing stress. Corresponding petrographic evidence is shown in Figs. 4g–h and S1e–f.

and 751 °C at 7 kbar and 9 kbar, respectively, consistent with the modelled upper temperature limit (Fig. 5). Retrograde metamorphism is interpreted to record decompression and cooling, based on the occurrence of chlorite and biotite around cracks in garnet and in the matrix.

6.1.2. Intermediate T/P metamorphism

Metabasites and metapelites from the eastern part of the Dengfeng Complex (MSU) have distinctive metamorphic characteristics compared with the migmatitic metabasite sample from the MBU. In the garnet-bearing amphibolite samples DF20-1-5 and 17DF22-2, the stability fields for the interpreted peak assemblages (Fig. 5) are consistent with intermediate T/P of ~ 510 – 600 °C/GPa. For garnet-free amphibolite sample DF10-1, the stability field for the interpreted peak assemblage extends over a large P – T range (Fig. 5), but is consistent with the P – T estimate based on HPq thermobarometry, and a T/P of around 560–580 °C/GPa. The prograde evolution of the samples is difficult to constrain, as there are no well-preserved inclusion assemblages and no clear compositional zoning in the garnet porphyroblasts. Retrograde metamorphism is interpreted to record decompression and cooling to greenschist facies conditions, presumably with some fluid influx, resulting in extensive chlorite growth.

For the three strongly-deformed metapelite samples (17DF20-6, 17DF20-1f, and DF12-7), the inferred peak assemblages are stable over a wide P – T range (Fig. 5). Calculated isopleths of Si (3.06–3.20, based on 11 oxygen atoms) in white mica (Table S1) more tightly constrain peak conditions to ~ 10 – 13 kbar at temperatures of ~ 550 – 655 °C, corresponding to intermediate T/P of ~ 425 – 590 °C/GPa. The prograde metamorphism of metapelite rocks is recorded in the inclusion assemblages in garnet porphyroblasts (Fig. 7a–c). In sample 17DF20-6, an inclusion assemblage of chloritoid–muscovite–chlorite–biotite–quartz–epidote–ilmenite in garnet cores (Figs. 4f and 7b) implies low- T , moderate- P conditions. Although chloritoid is not predicted in the pseudosection for sample 17DF20-6, it is predicted to be stable at pressures above 7.1 kbar and temperatures below 560 °C (Fig. 5) in an Al-rich sample (17DF20-1f) from the same outcrop. The garnet porphyroblasts record a sharp increase of X_{gr} from core (~ 0.08) to rim (~ 0.24) and a decrease in X_{gr} (0.24–0.17) at the rims, consistent

with a significant increase in pressure followed by decompression (Fig. S8a). Replacement of some rutile grains by ilmenite (Fig. 4d) is also consistent with decompression. The combined data suggest the metapelite samples followed a clockwise P – T path including a segment of near-isothermal decompression on the retrograde path, during which the rocks were strongly sheared to form widespread asymmetric S–C fabrics, boudins, and foliations (Fig. 7).

6.2. Timing of metamorphism

Zircon grains in the migmatitic tonalitic gneiss (LJG0201) from the western Part of the Dengfeng Complex record a crystallization age of 2528 ± 13 Ma (Fig. 6a) in the cores and a metamorphic recrystallization age of 2518 ± 12 Ma in the rims. Although these ages overlap within uncertainty, the latter is interpreted as the timing of anatexis of the TTG gneisses. Cores of zircon grains from the garnet amphibolite sample (17DF15-1) from the western part of the Dengfeng Complex have morphological and trace element characteristics consistent with an igneous origin, and define a $^{207}\text{Pb}/^{206}\text{Pb}$ age of 2537 ± 36 Ma (Fig. 6b), interpreted to record crystallization of the magmatic protolith. Analyses of zircon rims from the same sample, interpreted to be of metamorphic origin, yield a weighted mean $^{207}\text{Pb}/^{206}\text{Pb}$ age of 2500 ± 9 Ma (Fig. 6c), interpreted to date high- T metamorphism. These data are consistent with U–Pb analyses of titanite, which define a lower intercept age of 2501 ± 27 Ma (Fig. 6d), and existing data from samples of amphibolite and TTG gneiss from the region (Deng et al., 2016; Diwu et al., 2011; Huang et al., 2019; Wan et al., 2009). The early metamorphic episode in the western part of the Dengfeng Complex at ca. 2.52–2.50 Ga was associated with relatively high T/P as recorded in migmatitic TTG rocks and metabasites, which occurred shortly after the formation of their protoliths at ca. 2.54–2.52 Ga.

In the eastern part of the Dengfeng Complex (MSU), zircon grains in a garnet amphibolite sample (17DF22-2) define a discordia with an upper intercept age of 2532 ± 10 Ma (Fig. 6e), interpreted to reflect crystallisation age of the magmatic protolith. No metamorphic zircon rims are present in this sample. In a metapelite sample (17DF20-6) from the MSU, five analyses on rims of zircons yield a weighted mean $^{207}\text{Pb}/^{206}\text{Pb}$ age of 2504 ± 16 Ma (Fig. 6f), interpreted as the time of metamorphism affecting

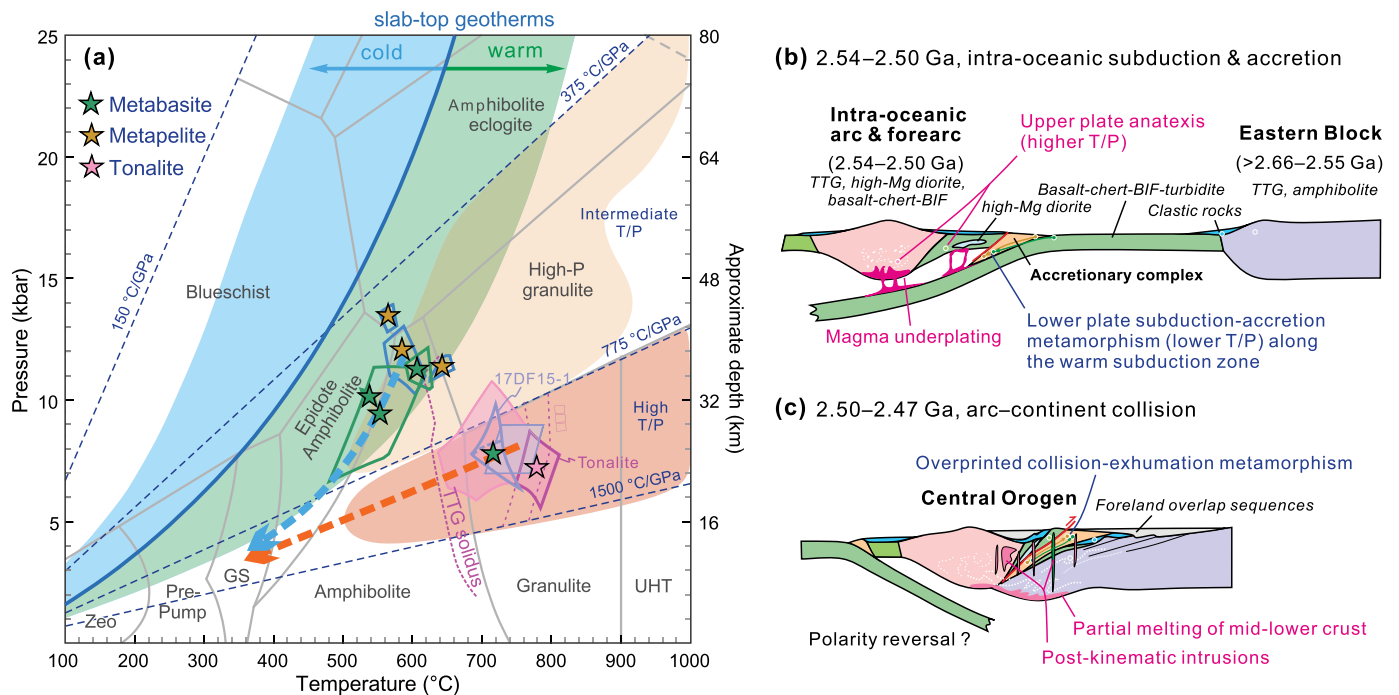


Fig. 8. Summary of peak P - T conditions and the geodynamic model. (a) The peak metamorphic P - T conditions recorded in the metapelites and metabasites from the eastern part of the Dengfeng Complex are consistent with intermediate thermobaric ratios, whereas the metabasite and tonalitic gneiss in the west are consistent with high apparent geothermal gradients. The former is similar to slab-top geotherms of Neoproterozoic to Phanerozoic subduction zones (blue solid lines and shaded area) compiled by Penniston-Dorland et al., 2015. The metamorphic facies were modified from Hernández Uribe and Palin (2019). Intermediate and high T/P fields (yellow and brown, respectively) were based on the global metamorphic database (Brown and Johnson, 2018). (b) Intra-oceanic subduction and forearc accretion at ca. 2.54–2.50 Ga. The upper plate arc-forearc with relatively higher geotherms records intense anatexis in the TTG and metabasites due to magma underplating, whereas the accretionary complex with lower T/P metamorphism was formed along the lower-geotherm subduction zone, corresponding to “warm” subduction zones in the Phanerozoic. See text for details. (c) Arc-continent collision at ca. 2.50–2.47 Ga. The collisional event likely resulted in extensive deformation and further anatexis of TTG suites and amphibolites at the initial stage of collision at ca. 2.50 Ga, with subsequent intrusion of potassic felsic plutons/dikes that were probably derived from partial melting of former granitic rocks at ca. 2.50–2.42 Ga, and coeval mafic dikes. At ca. 2.45 Ga the newly-assembled Dengfeng Complex was unconformably overlain by the Paleoproterozoic Songsshan Group, which is interpreted as a foreland clastic wedge. During exhumation, the Dengfeng Complex underwent retrograde greenschist facies metamorphism.

the metapelites. Importantly, the youngest detrital zircon grain (ca. 2.45 Ga) from the basal conglomerate of the overlying greenschist facies Paleoproterozoic Songsshan Group (Wan et al., 2009), and widespread post-kinematic plutons and dikes with ages ranging from ca. 2.50 Ga to 2.40 Ga (Deng et al., 2019; Huang et al., 2019; Zhou et al., 2011), provide an upper limit for metamorphism at ca. 2.50 Ga.

In summary, our new data, together with existing age data, indicate that the metavolcano-sedimentary rocks in the Dengfeng granite-greenstone belt underwent peak metamorphism at 2.52–2.50 Ga. On a regional scale (Fig. 1b), evidence in support of a late Neoproterozoic to early Paleoproterozoic (ca. 2.52–2.46 Ga) amphibolite-granulite facies metamorphic episode in the NCC is growing (e.g., Liu et al., 2015; Wang et al., 2019; Zhang et al., 2020). These new data from the NCC indicate that metamorphism was characterized by moderate- to high- T/P peak conditions, with the diversity of P - T paths reflecting metamorphism in different tectonothermal environments.

6.3. Implications for the Neoproterozoic arc-continent collision of the NCC

As discussed above, two Neoproterozoic (ca. 2.52–2.50 Ga) metamorphic zones with distinct thermobaric ratios are recognized in the Dengfeng Complex with a higher T/P metamorphic zone (~720–1400 °C/GPa) in the west, and an intermediate T/P (~425–600 °C/GPa) metamorphic zone in the east (Fig. 8a). Our data reveal the contemporaneous occurrence of two contrasting types of metamorphism and a duality of thermal regimes. High T/P (>775 °C/GPa) metamorphism is generally developed in the hinterland of an overriding plate, whereas intermediate and low

T/P (<775 °C/GPa) metamorphism, at least since the Neoproterozoic, is commonly associated with subduction and collisional settings (e.g., Brown and Johnson, 2018). Consequently, we suggest that the ca. 2.54–2.51-Ga Dengfeng granite-greenstone belt can be interpreted as a remnant of a spatially and temporally linked Neoproterozoic paired metamorphic belt recording subduction to collisional orogenesis at a convergent plate margin (Fig. 8b).

This interpretation is consistent with recent structural and geochemical data. Based on the N-MORB and IAT affinities of the metabasaltic rocks, which are associated with coeval sanukitoid-like high-Mg metadiorite and adakitic granitic sills, the MBU is interpreted to have formed in a subduction-related forearc setting (Huang et al., 2019). The ca. 2.54–2.51 Ga TTG rocks, high-Mg metadiorite, and metabasalt-BIF-chert sequences in the western part of the Dengfeng Complex are collectively interpreted as an intra-oceanic arc and forearc assemblage in the upper plate. The heat sourced from underplating of mantle-derived magma or possible ridge subduction beneath the arc-forearc region might have induced intense anatexis and high T/P metamorphism of deeper arc-forearc rocks associated with high geothermal gradients (Fig. 8b).

By contrast, in the eastern Dengfeng Complex, the MSU contains coherent and chaotic units including greenschist-amphibolite facies schist-metabasite assemblages, metaturbidite, and block-in-matrix mélanges that resembles an accretionary complex (dismembered ocean plate stratigraphy), as preserved in many Phanerozoic orogenic belts (Kusky et al., 2018). Based on detailed field mapping and structural data, Huang et al. (2019) proposed that the MSU represents a subduction-accretion complex, which records a complex history involving underplating, off-scraping and fragmenta-

tion of the oceanic plate stratigraphy (basalt–chert–shale–BIF, and trench-fill turbidites) in the subducting plate, and incorporation of exotic suprasubduction zone-type mafic blocks into the mélanges. Kinematic indicators, including mineral and stretching lineations and asymmetric fabrics, indicate a top-to-the-northeast transport direction (Huang et al., 2019).

Inclusions of chloritoid-bearing mineral assemblages in garnet porphyroblasts within metapelites reflect a relatively cool thermal gradient during the early stages of accretionary orogenesis. The compositions of garnet rims and Si contents of white mica are consistent with significant burial to pressures exceeding 10 kbar, corresponding to a depth of at least 30 km assuming lithostatic pressure (Fig. 8a). Metabasic blocks within the mélange preserve variable mineral assemblages and peak P – T conditions, which are common features in Phanerozoic accretionary wedges in which a variety of greenschist to eclogite facies tectonic blocks are preserved in a single belt due to exhumation from different depths in the subduction channel (Cloos and Shreve, 1988). The accretionary complex was probably modified by a subsequent arc–continent collision event, resulting in further shearing and a significant increase of pressure at relatively low temperature, as recorded by asymmetric shear fabrics and the rim compositions of garnet porphyroblasts (Fig. 7d–f). The overall peak P – T conditions of the metabasites and metapelites in the MSU are consistent with the slab-top geotherms from ‘warm’ subduction zones (Fig. 8a), as reconstructed based on maximum P – T conditions of exhumed Neoproterozoic–Phanerozoic subduction zone rocks (dominantly blueschists and eclogites) from global orogens and accretionary wedges (Penniston-Dorland et al., 2015). Therefore, the P – T evolution of the metapelites and metabasites is consistent with subduction and collision during which they were buried to >30 km and underwent intense shearing and metamorphism within a warm subduction zone (Fig. 8b).

The timing of initial arc–continent collision is constrained at ca. 2.50 Ga based on existing data and the new data presented here (Deng et al., 2019; Diwu et al., 2011; Huang et al., 2019; Wang et al., 2017; Zhou et al., 2011). The younger partial melting events recorded in the potassic intrusions (ca. 2.42 Ga) and leucogranitic veins in high-Mg metadiorite (ca. 2.47 Ga), and the numerous post-kinematic felsic and mafic dikes (ca. 2.50–2.40 Ga), probably resulted from crustal thickening and subsequent extension during arc–continent collision (Fig. 8c). The arc–continent collision and tectonic stacking of different units took place prior to ca. 2.50 Ga, and the assembled Dengfeng Complex was exhumed prior to ca. 2.45 Ga, before erosion and sedimentation of the overlying lower Songshan Group, which is interpreted as a foreland succession (Huang et al., 2019; Kusky et al., 2016). Paleoproterozoic metamorphism at ca. 1.95–1.80 Ga overprinted most regions across the NCC (Kusky et al., 2016), but it is not significantly recorded by rocks in the Dengfeng Complex (Wan et al., 2009; Wang et al., 2017; Huang et al., 2019).

A model of west-directed intra-oceanic subduction, forearc accretion (ca. 2.54–2.50 Ga), and subsequent arc–continent collision (ca. 2.50–2.47 Ga) can viably explain the age variations, structural relationships, metamorphic patterns, geochemical characteristics, and spatial configurations of the different lithostructural units of the Dengfeng granite–greenstone belt (Fig. 8b, c). The accretion of intra-oceanic arc(s) to the eastern NCC reflect the early episode of accretionary-to-collisional orogenesis along the Central Orogenic Belt (Fig. 1b).

6.4. Implications for the Neoproterozoic tectonic regime

The global tectonic regime in the Neoproterozoic is a matter of debate. Recent reviews suggest that a significant change in the average composition of continental crust (from mafic to more felsic)

and metamorphic patterns (paired metamorphism) might have occurred during the Meso- to Neoproterozoic (ca. 3.2–2.5 Ga), which may or may not reflect the emergence of global plate tectonics from some earlier tectonic mode(s) (e.g., Cawood et al., 2018; Johnson et al., 2019; Moya and Laurent, 2018). However, low T/P metamorphic rocks that characterise Neoproterozoic–Phanerozoic subduction-accretionary complexes (e.g., Stern, 2018) have not yet been found in the Archean rock record, consistent with suggested higher geothermal gradients and mantle potential temperatures at that time (Aulbach and Arndt, 2019; Herzberg et al., 2010), or a lack of preservation (Brown and Johnson, 2019; Brown et al., 2020).

The recognition of a remnant Neoproterozoic paired metamorphic belt in the Dengfeng Complex indicates subduction-collision processes were operating at the end of the Archean in the NCC, and potentially were widespread based on the paucity of preservation of paired metamorphic belts in the modern plate mosaic. Significantly, the medium T/P metamorphism recorded in the accretionary segment of the eastern Dengfeng Complex is broadly in line with ‘warm’ slab-top geotherms of the Neoproterozoic–Phanerozoic subduction zones around the world (Fig. 8a) (Penniston-Dorland et al., 2015), consistent with warmer geotherms associated with Neoproterozoic subduction zones, which might be related to the more common subduction of young (<30 Ma in this case) and warm oceanic slabs (e.g., van Keken et al., 2018), as well as higher mantle temperatures. The secular evolution in the patterns of paired metamorphism from intermediate–high T/P in the Neoproterozoic to widespread low/intermediate–high T/P in the Phanerozoic (minor in Paleoproterozoic) is likely a manifestation of secular cooling of the mantle and the associated styles of plate tectonics (e.g., Brown et al., 2020; Holder et al., 2019; Kusky, 2020; Zheng and Zhao, 2020).

This study, together with a recent structural synthesis (Huang et al., 2019), highlights the complexity of individual granite–greenstone belts in terms of metamorphism, structure, and geochemistry. The combination of detailed field, geochemical, geochronological, structural and metamorphic data thus permits recognition of convergent margin processes in some Archean granite–greenstone belts.

7. Conclusions

(1) Zircon and titanite U–Pb dating reveal that the TTG and volcano-sedimentary rocks in the Dengfeng Complex have metamorphic ages of ca. 2.52–2.50 Ga.

(2) Two distinct but structurally, spatially, and temporally paired metamorphic belts are recognized: a higher T/P belt in the western part of the Dengfeng Complex, characterized by intense partial melting of TTG gneisses and amphibolites, contrasting with a medium T/P metamorphic belt with strongly-deformed metapelites and amphibolites in the eastern part of the Dengfeng Complex (MSU). The peak P – T conditions in the medium T/P metamorphic belt are consistent with the slab-top geotherms of ‘warm’ subduction zones in the Neoproterozoic to Phanerozoic.

(3) A model of intra-oceanic subduction, fore-arc accretion, and arc–continent collision viably accounts for the observed structural, geochemical, and metamorphic characteristics of the ca. 2.54–2.50-Ga Dengfeng Complex.

(4) Recognition of the relicts of a Neoproterozoic paired metamorphic belt in the southern NCC supports the operation of plate tectonics at the end of the Archean.

Declaration of competing interest

The authors declare that they have no known competing financial interests or personal relationships that could have appeared to influence the work reported in this paper.

Acknowledgements

We are grateful to Chun-Ming Wu, Alex Webb, and an anonymous reviewer for their very helpful and constructive reviews, and An Yin for his efficient editorial handling. We thank Noreen Evans, Brad MacDonald, and Adam Frew (Curtin University) for help with zircon and titanite dating. This work was supported by the National Natural Science Foundation of China (41572203, 41890834), the 111 Project of the Ministry of Education of China (BP0719022), the MOST Special Fund (MSFGPMR02-3) and the Open Fund (GPMR201704, and GPMR201903) from the State Key Laboratory of Geological Processes and Mineral Resources, China University of Geosciences, Wuhan, and the Fundamental Research Funds for National Universities from the China University of Geosciences, Wuhan. A. Polat acknowledges support from the China University of Geosciences, Wuhan and the Natural Sciences and Engineering Research Council of Canada (Discovery Grant RGPIN-2019-04236). This is a contribution to the China Scholarship Council projects awarded to B. Huang and D. Fu.

Appendix A. Supplementary material

Supplementary material related to this article can be found online at <https://doi.org/10.1016/j.epsl.2020.116355>.

References

- Arndt, N.T., 2013. The formation and evolution of the continental crust. *Geochem. Perspect.* 2 (3), 405–533.
- Aulbach, S., Arndt, N.T., 2019. Eclogites as palaeodynamic archives: evidence for warm (not hot) and depleted (but heterogeneous) Archaean ambient mantle. *Earth Planet. Sci. Lett.* 505, 162–172.
- Bédard, J.H., 2018. Stagnant lids and mantle overturns: implications for Archaean tectonics, magmatogenesis, crustal growth, mantle evolution, and the start of plate tectonics. *Geosci. Front.* 9 (1), 19–49.
- Brown, M., 2010. Paired metamorphic belts revisited. *Gondwana Res.* 18 (1), 46–59.
- Brown, M., Johnson, T., 2018. Secular change in metamorphism and the onset of global plate tectonics. *Am. Mineral.* 103 (2), 181–196.
- Brown, M., Johnson, T., 2019. Metamorphism and the evolution of subduction on Earth. *Am. Mineral.* 104 (8), 1065–1082.
- Brown, M., Johnson, T., Gardiner, N.J., 2020. Plate tectonics and the Archaean Earth. *Annu. Rev. Earth Planet. Sci.* 48 (1). <https://doi.org/10.1146/annurev-earth-081619-052705>.
- Cawood, P.A., Hawkesworth, C.J., Pisarevsky, S.A., Dhuime, B., Capitanio, F.A., Nebel, O., 2018. Geological archive of the onset of plate tectonics. *Philos. Trans. R. Soc. A* 376 (2132), 20170405.
- Cloos, M., Shreve, R.L., 1988. Subduction-channel model of prism accretion, melange formation, sediment subduction, and subduction erosion at convergent plate margins: 1. Background and description. *Pure Appl. Geophys.* 128 (3–4), 455–500.
- Deng, H., Kusky, T., Polat, A., Wang, C., Wang, L., Li, Y., Wang, J., 2016. A 2.5 Ga fore-arc subduction-accretion complex in the Dengfeng Granite-Greenstone Belt, Southern North China Craton. *Precambrian Res.* 275, 241–264.
- Deng, H., Kusky, T., Polat, A., Lan, B., Huang, B., Peng, H., Wang, J., Wang, S., 2019. Magmatic record of Neoproterozoic arc-polarity reversal from the Dengfeng segment of the Central Orogenic Belt, North China Craton. *Precambrian Res.* 326, 105–123.
- Diwu, C., Sun, Y., Guo, A., Wang, H., Liu, X., 2011. Crustal growth in the North China Craton at ~2.5 Ga: evidence from in situ zircon U–Pb ages, Hf isotopes and whole-rock geochemistry of the Dengfeng complex. *Gondwana Res.* 20 (1), 149–170.
- François, C., Debaille, V., Paquette, J., Baudet, D., Javaux, E.J., 2018. The earliest evidence for modern-style plate tectonics recorded by HP–LT metamorphism in the Paleoproterozoic of the Democratic Republic of the Congo. *Sci. Rep.* 8 (1).
- Ganne, J., De Andrade, V., Weinberg, R.F., Vidal, O., Dubacq, B., Kagambega, N., Naba, S., Baratoux, L., Jessell, M., Allibon, J., 2011. Modern-style plate subduction preserved in the Palaeoproterozoic West African craton. *Nat. Geosci.* 5 (1), 60–65.
- Glassley, W.E., Korstgard, J.A., Sorensen, K., Platou, S.W., 2014. A new UHP metamorphic complex in the 1.8 Ga Nagssugtoqidian Orogen of West Greenland. *Am. Mineral.* 99 (7), 1315–1334.
- Green, E.C.R., White, R.W., Diener, J.F.A., Powell, R., Holland, T.J.B., Palin, R.M., 2016. Activity-composition relations for the calculation of partial melting equilibria in metabasic rocks. *J. Metamorph. Geol.* 34 (9), 845–869.
- Hayden, L.A., Watson, E.B., Wark, D.A., 2008. A thermobarometer for sphene (titanite). *Contrib. Mineral. Petrol.* 155 (4), 529–540.
- Hernández Uribe, D., Palin, R.M., 2019. A revised petrological model for subducted oceanic crust: insights from phase equilibrium modelling. *J. Metamorph. Geol.* 37 (6), 745–768.
- Herzberg, C., Condie, K., Korenaga, J., 2010. Thermal history of the Earth and its petrological expression. *Earth Planet. Sci. Lett.* 292 (1–2), 79–88.
- Holder, R.M., Viete, D.R., Brown, M., Johnson, T.E., 2019. Metamorphism and the evolution of plate tectonics. *Nature* 572 (7769), 378–381.
- Holland, T.J.B., Powell, R., 2011. An improved and extended internally consistent thermodynamic dataset for phases of petrological interest, involving a new equation of state for solids. *J. Metamorph. Geol.* 29 (3), 333–383.
- Huang, B., Kusky, T., Wang, L., Polat, A., Fu, D., Windley, B., Deng, H., Wang, J., 2019. Structural relationships and kinematics of the Neoproterozoic Dengfeng forearc and accretionary complexes, southern North China craton. *Geol. Soc. Am. Bull.* 131 (5–6), 966–996.
- Johnson, T.E., Brown, M., Kaus, B.J.P., VanTongeren, J.A., 2014. Delamination and recycling of Archaean crust caused by gravitational instabilities. *Nat. Geosci.* 7 (1), 47–52.
- Johnson, T.E., Kirkland, C.L., Gardiner, N.J., Brown, M., Smithies, R.H., Santosh, M., 2019. Secular change in TTG compositions: implications for the evolution of Archaean geodynamics. *Earth Planet. Sci. Lett.* 505, 65–75.
- Korenaga, J., 2013. Initiation and evolution of plate tectonics on Earth: theories and observations. *Annu. Rev. Earth Planet. Sci.* 41 (1), 117–151.
- Kröner, A., Compston, W., Zhang, G., Guo, A., 1988. Age and tectonic setting of Late Archaean greenstone-gneiss terrain in Henan Province, China, as revealed by single-grain zircon dating. *Geology* 16, 211–215.
- Kusky, T., 2020. Plate tectonics in relation to mantle temperatures and metamorphic properties. *Sci. China Earth Sci.* 63 (5), 634–642.
- Kusky, T.M., Polat, A., 1999. Growth of granite-greenstone terranes at convergent margins, and stabilization of Archaean cratons. *Tectonophysics* 305 (1–3), 43–73.
- Kusky, T.M., Windley, B.F., Polat, A., 2018. Geological evidence for the operation of plate tectonics throughout the Archaean: records from Archaean paleo-plate boundaries. *J. Earth Sci.* 29 (6), 1291–1303.
- Kusky, T.M., Polat, A., Windley, B.F., Burke, K.C., Dewey, J.F., Kidd, W.S.F., Maruyama, S., Wang, J.P., Deng, H., Wang, Z.S., Wang, C., Fu, D., Li, X.W., Peng, H.T., 2016. Insights into the tectonic evolution of the North China Craton through comparative tectonic analysis: a record of outward growth of Precambrian continents. *Earth-Sci. Rev.* 162, 387–432.
- Liu, S., Jahn, B., Wan, Y., Xie, H., Wang, S., Xie, S., Dong, C., Ma, M., Liu, D., 2015. Neoproterozoic to Paleoproterozoic high-pressure mafic granulite from the Jiaodong Terrain, North China Craton: petrology, zircon age determination and geological implications. *Gondwana Res.* 28 (2), 493–508.
- Miyashiro, A., 1961. Evolution of metamorphic belts. *J. Petrol.* 2 (3), 277–311.
- Moyen, J., Laurent, O., 2018. Archaean tectonic systems: a view from igneous rocks. *Lithos* 302–303, 99–125.
- Penniston-Dorland, S.C., Kohn, M.J., Manning, C.E., 2015. The global range of subduction zone thermal structures from exhumed blueschists and eclogites: rocks are hotter than models. *Earth Planet. Sci. Lett.* 428, 243–254.
- Polat, A., Wang, L., Appel, P.W.U., 2015. A review of structural patterns and melting processes in the Archaean craton of West Greenland: evidence for crustal growth at convergent plate margins as opposed to non-uniformitarian models. *Tectonophysics* 662, 67–94.
- Powell, R., Holland, T.J.B., 1988. An internally consistent dataset with uncertainties and correlations: 3. Applications to geobarometry, worked examples and a computer program. *J. Metamorph. Geol.* 6 (2), 173–204.
- Sizova, E., Gerya, T., Stüwe, K., Brown, M., 2015. Generation of felsic crust in the Archaean: a geodynamic modeling perspective. *Precambrian Res.* 271, 198–224.
- Smithies, R.H., Ivanic, T.J., Lowrey, J.R., Morris, P.A., Barnes, S.J., Wyche, S., Lu, Y., 2018. Two distinct origins for Archaean greenstone belts. *Earth Planet. Sci. Lett.* 487, 106–116.
- Stern, R.J., 2018. The evolution of plate tectonics. *Philos. Trans. R. Soc. A* 376 (2132), 20170406.
- Sun, S., McDonough, W.F., 1989. Chemical and isotopic systematics of oceanic basalts: implications for mantle composition and processes. *Geol. Soc. (Lond.) Spec. Publ.* 42 (1), 313–345.
- Tang, M., Chen, K., Rudnick, R.L., 2016. Archaean upper crust transition from mafic to felsic marks the onset of plate tectonics. *Science* 351 (6271), 372–375.
- Turner, S., Wilde, S., Wörner, G., Schaefer, B., Lai, Y., 2020. An andesitic source for Jack Hills zircon supports onset of plate tectonics in the Hadean. *Nat. Commun.* 11 (1).
- van Keken, P.E., Wada, I., Abers, G.A., Hacker, B.R., Wang, K., 2018. Mafic high-pressure rocks are preferentially exhumed from warm subduction settings. *Geochem. Geophys. Geosyst.* 19 (9), 2934–2961.
- Van Kranendonk, M.J., Kröner, A., Hoffmann, J.E., Nagel, T., Anhaeusser, C.R., 2014. Just another drip: re-analysis of a proposed Mesoproterozoic suture from the Barberton Mountain Land, South Africa. *Precambrian Res.* 254, 19–35.
- Wan, Y., Liu, D.Y., Wang, S.Y., Zhao, X., Dong, C.Y., Zhou, H.Y., Yin, X.Y., Yang, C.X., Gao, Z.L., 2009. Early Precambrian crustal evolution in the Dengfeng area, Henan province (eastern China): constraints from geochemistry and SHRIMP U–Pb zircon dating. *Acta Geol. Sin.* 83 (7), 982–999.

- Wang, X., Huang, X., Yang, F., Luo, Z., 2017. Late Neoproterozoic magmatism and tectonic evolution recorded in the Dengfeng Complex in the southern segment of the Trans-North China Orogen. *Precambrian Res.* 302, 180–197.
- Wang, C., Song, S., Allen, M.B., Su, L., Wei, C., 2019. High-pressure granulite from Jixian, Eastern Hebei, the North China Craton: implications for Neoproterozoic to early Paleoproterozoic collision tectonics. *Geol. Soc. (Lond.) Spec. Publ.* 478 (1), 427–448.
- Webb, A.A.G., Müller, T., Zuo, J., Haproff, P.J., Ramírez-Salazar, A., 2020. A non-plate tectonic model for the Eoarchean Isua supracrustal belt. *Lithosphere* 12 (1), 166–179.
- Weller, O.M., St-Onge, M.R., 2017. Record of modern-style plate tectonics in the Paleoproterozoic Trans-Hudson orogen. *Nat. Geosci.* 10 (4), 305–311.
- White, R.W., Powell, R., Holland, T.J.B., Johnson, T.E., Green, E.C.R., 2014. New mineral activity-composition relations for thermodynamic calculations in metapelitic systems. *J. Metamorph. Geol.* 32 (3), 261–286.
- Wu, C.M., Zhang, J., Ren, L.D., 2004. Empirical garnet-biotite-plagioclase-quartz (GBPQ) geobarometry in medium- to high-grade metapelites. *J. Petrol.* 45 (9), 1907–1921.
- Xu, C., Kynický, J., Song, W., Tao, R., Lü, Z., Li, Y., Yang, Y., Pohanka, M., Galiova, M.V., Zhang, L., Fei, Y., 2018. Cold deep subduction recorded by remnants of a Paleoproterozoic carbonated slab. *Nat. Commun.* 9 (1), 2790.
- Zhang, G., Bai, Y., Sun, Y., Guo, A., Zhou, D., Li, T., 1985. Composition and evolution of the Archaean crust in central Henan, China. *Precambrian Res.* 27 (1–3), 7–35.
- Zhang, H.C.G., Peng, T., Liu, J., Wang, J., Chen, Y., Zhang, Q.W.L., Wu, C., 2020. New geochronological evidences of late Neoproterozoic and late Paleoproterozoic tectono-metamorphic events in the Miyun area, North China Craton. *Precambrian Res.* 345, 105774.
- Zhao, G., Sun, M., Wilde, S.A., Li, S., 2005. Late Archean to Paleoproterozoic evolution of the North China Craton: key issues revisited. *Precambrian Res.* 136 (2), 177–202.
- Zheng, Y., Zhao, G., 2020. Two styles of plate tectonics in Earth's history. *Sci. Bull.* 65 (4), 329–334.
- Zhou, Y., Zhao, T., Wang, C.Y., Hu, G., 2011. Geochronology and geochemistry of 2.5 to 2.4 Ga granitic plutons from the southern margin of the North China Craton: implications for a tectonic transition from arc to post-collisional setting. *Gondwana Res.* 20 (1), 171–183.